Research Article ISSN 2639-9512

Stem Cell & Regenerative Medicine

Plain and Stromal Cells Seeded Collagen Nanofibers Promote Bone Regeneration *In vivo*. A Rat Calvaria Defect Model

Bou-Akl Therese[1], Wu Bin[2], Daly-Seiler Conor[2], Dietz Paula[2], Ren Weiping[1] and Markel David[3]

[1]*Ascension Providence Hospital, Wayne State University, United States.*

[2]*Ascension Providence Hospital, United States.*

[3]*Ascension Providence Hospital, The Core Institute Michigan, United States.*

***Correspondence:**
Therese Bou-Akl MD, PhD, 16001 West Nine Mile Road, Southfield, United States, Tel: 248-849-2564; Fax: 248-849-5366.

Received: 02 May 2020; **Accepted:** 31 May 2020

Citation: Bou-Akl Therese, Wu Bin, Daly-Seiler Conor, et al. Plain and Stromal Cells Seeded Collagen Nanofibers Promote Bone Regeneration *In vivo*. A Rat Calvaria Defect Model. Stem Cells Regen Med. 2020; 4(1): 1-7.

ABSTRACT

The limitations of commonly used bone graft materials have encouraged testing of tissue engineered graft materials. We evaluated electrospun collagen nanofibers (CNFs) alone and in combination with bone marrow stromal cells (BMSCs) as new bone graft biomaterials using a rat calvarial critical defect model, empty defects were used as control. Our hypotheses were: 1) CNFs will isolate the defect from the surrounding tissue and prevent its filling with fibrotic tissue 2) CNFs and BMSCs will further promote osteogenesis and lead to more organized bone repair. Healing was evaluated by microcomputed tomography (MicroCT) at 0, 6, 12 and 16 weeks. Bone volume fraction (BVF) analyzed. Renderings of defects used to grade bony bridging. At 16 weeks, animals sacrificed and the defects with surrounding bone removed, fixed, decalcified and processed for histology. Stained sections assessed for type and maturity of new bone. Increased bone filling was observed in the two experimental groups. Histology showed that CNFs alone and CNFs + BMSCs minimized fibrotic tissue invasion and promoted bone regeneration. Significant difference was found in BVF and bony bridging only between control and the CNF. Our results indicate CNFs with and without BMSCs can provide favorable stimulus for bone regeneration.

Keywords

Bone regeneration, Calvarial defect, Collagen, Nanofibers, Stromal cells.

Introduction

As the complexity of prosthetic orthopaedic and maxillofacial surgeries advance the need for bone augmentation at the implant sites is increasing. When restoration of the anatomy requires filling a bony defect, surgeons usually utilize bone autografts and allografts. These types of grafts are associated with donor site morbidity [1,2] and graft resorption or collapse [3-5]. Instead of using bone grafts surgeons are increasingly looking to resorbable or non-resorbable bone graft substitutes.

Tissue engineered bone graft substitute materials are attractive alternatives to synthetic grafts since they are biocompatible, bioactive and designed to degrade after the appropriate native cells start making their own matrix. Collagen is an abundant protein and is a critical structural component of bone. Collagen meets all the desired criteria for an applicable biomaterial as it is extensively involved in the process of adhesion and proliferation of many cell types. Collagen possess physicochemical properties that can be modified by crosslinking since it has amino, carboxyl and hydroxyl groups that serve as crosslinking sites [6]. The Brunel group investigated the effect of crosslinking collagen on the repair of calvaria defects in rat model and showed that crosslinking delayed the resorption of collagen membranes, supporting the feasibility of these membranes as guided bone regeneration (GBR) materials. Surprisingly, the amount of crosslinking did not appear to influence the outcomes in that study [7].

Stem cell therapy is becoming a mainstay for bone tissue engineering due to its proven pluripotent nature and ability to stimulate osteogenic repair in vitro and *in vivo*. Rat bone marrow stromal cells (BMSCs) are multi-potent and are characterized in vitro by their ability to differentiate into osteogenic, chondrogenic, and adipogenic phenotypes [8-10]. After isolation these cells retain their self-renewal and differentiation capacity. George and Miyata showed that in addition to the composition of the extracellular matrix, the structure of the scaffolding material appears to play an important role in promoting the growth and differentiation of BMSCs. Their rat BMSCs differentiated into

osteoblasts on honeycomb collagen scaffold without the addition of other differentiation factors [10]. Rochefort in 2016 further showed that the use of collagen gel seeded with dental pulp stem cells significantly accelerated the bone regeneration of rat calvarial defects [11]. In our previous work, we tested the differentiation capability of BMSCs on collagen nanofiber matrices without the use of additional differentiation factors. After five weeks of culture the BMSCs differentiated into osteoblasts and showed the ability to deposit calcium minerals on the material surface [12].

In normal bone the collagen fibers orientation plays an important role in the mechanical stability. Studies done in 1967 by Ascenzi and 1973 by Evans showed that the predominant direction of the collagen fibers is about the osteon's long axis leading to increase in the ultimate tensile strength and strain of the bone [13,14]. The effect of crosslinking and crosslinking agents on the mechanical properties of collagen fibers have been studied by many investigators like Kato [15], Olde Damink [16], Caruso [17] and our group [18]. Those studies have shown that crosslinking considerably improved the mechanical properties of collagen fibers. For this *in vivo* study, we used optimized collagen nanofiber sheets with optimized crosslinking conditions.

The objective of this study was to evaluate the effect of collagen nanofiber sheets alone and in combination with rat BMSCs on bone regeneration *in vivo*. We hypothesized that a biomaterial consisting of aligned, crosslinked collagen nanofiber sheets and differentiated BMSCs would be superior to the control and to the sheets without BMSCs in promoting osteogenesis and thus lead to more organized bone repair.

Materials and Methods

Nanofiber sheets fabrication and crosslinking

Type I collagen from rat-tail tendons was isolated using the method of Elsdale [19]. The collagen was used to form collagen nanofibers as follows. The lyophilized dry collagen at a concentration of 12% w/v was dissolved in 2.45ml of Hexafluoro-2-propanol (HFP) and 0.05ml of deionized water. The protocol for obtaining electrospun aligned nanofibers was based on the work of Matthews and Heiden using a custom apparatus [20,21]. The electrospun nanofibers were crosslinked following the method by Caruso and Dunn [17] using 1-ethyl-3-(3-dimethylaminopropyl) carbodiimide hydrochloride (EDC) in acetone and detailed in our previous publications [12,18]. Crosslinked sheets were sterilized in 70% ethanol for 24 hours, then washed with sterile distilled water four times. Sterile sheets were stored in sterile phosphate buffer saline at 4ºC. Circular discs measuring 10mm in diameter and 0.2mm thickness were punched out form the nanofiber collagen sheets and prepared for implantation.

BMSCs isolation and culture

BMSCs from Fisher 344 rats were isolated using an established method [22]. The rat femurs were dissected free and both proximal and distal ends removed leaving the diaphyseal shaft. the shafts were flushed with Dulbecco's Modified Eagles Medium (DMEM) containing 10% Fetal Bovine Serum (FBS), penicillin 20 mU/ml and streptomycin 20 µg/ml using an 18-gauge needle, the cell suspension was passed through a 70-µm nylon cell strainer. The cell suspension was plated in 25 cm^2 tissue culture flasks and incubated at 37ºC and 5% CO_2. The first medium change was done after three days and then every other day (7-10days) until the adherent cells reached 70% confluency, then those were trypsinized and subcultured at a ratio of 1:3. Cells used in this experiment were from passage four. Twelve discs were directly seeded with BMSCs at a density of 1x 10^6 cells per cm^2 in 100µl of medium and cultured for 3 weeks before implantation.

Animal Surgery

All animal work was performed in compliance with institutional committee guidelines for animal welfare. Critical bone defects were created in the calvariae of 18 male Fisher 344 rats following the protocol of Spicer et al. [23] Animals anesthesia was induced using isoflurane 5% in oxygen for 2 min then anesthesia maintained with 1-3% isoflurane in oxygen for the duration of the surgery. A 1.5 cm midline incision was made down to the scalp periosteum from the nasal bone to just caudal to the bregma. The periosteum covering of the calvarium was divided and pushed laterally to expose the underlying bone, then the calvarium scored with surgical drill and trephine at 1500 rpm with constant irrigation of sterile normal saline. The trephinated portion of bone was lifted using a periosteal elevator creating an 8 mm diameter, full thickness, round critical calvarial defect. Special attention was made to prevent injuries to the periosteum or the dura during the surgery (Figure 1). The defect was left either untreated (G1- negative control, n=6), was repaired using unseeded collagen nanofiber discs (G2, n=6), or repaired using BMSCs seeded discs (G3, n=6). In the G2 animals, the defects were closed by implanting one nanofiber disc under and one nanofiber disc on top of the defect to create a sandwich like construct. In the G3 animals, a similar "sandwich" was made using seeded discs with the cell seeded sides facing inwards to the space created between the two discs.

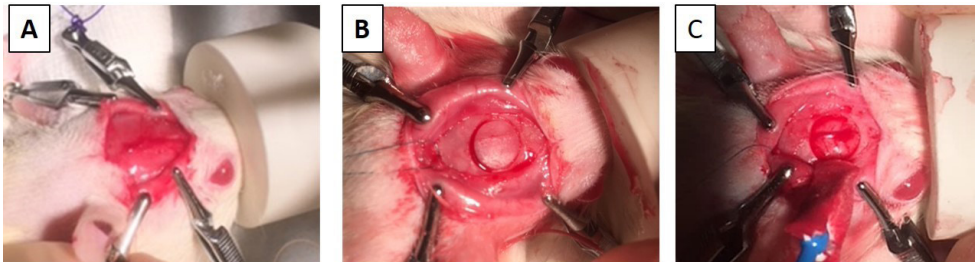

Figure 1: Shows the surgical steps for the creation of critical defect: Skin incision (A), pushing the periosteum to the sides and drilling the 8mm circle(B), removal of the drilled bone and showing the intact underlying tissue(C).

Before closing the cranial incision, intraperitoneal injections of 0.05 mg/kg buprenorphine were given. The periosteum was approached and closed using a 5-0 absorbable (Monocryl) suture and the skin was closed with size 4-0 of the same type of sutures. After the surgery animals were housed individually and provided with food and water ad libitum. Ketoprofen 5mg/kg was administered post-operatively and once daily for one week after assessment of the animals.

The surgical site (head) was scanned using Micro Computed Tomography (micro-CT) at four-time points: zero time (within 48hrs of surgery), at 6 weeks, 12 weeks and at 16 weeks after the surgery. The animals were sacrificed 16 weeks after surgery. Gross images of the retrieved bones with the defect where taken before sample fixation and the defects were further assessed post mortem using histological methods.

Micro Computed Tomography

Animals were anesthetized using isoflurane 4% in oxygen for induction then placed in a holder headfirst with 1-3% continuous isoflurane in oxygen for the duration of the scan (~45 minutes). MicroCT imaging was performed using a Scanco MicroCT scanner (VivaCT 40; Scanco Medical AG, Bassersdorf, Switzerland) with an x-ray source power of 70 kVp and 114 µA MAS. Scans varied from 8.4 µm to 11.2 µm in length and were collected in 21.0 µm slice increments, yielding a voxel size of 21.0 µm (maximum resolution was not utilized to minimize the time animals spent under anesthesia). To reduce noise, the scanned grayscale images were filtered through a low-pass Gaussian filter (sigma = 0.8, support = 1). Data was collected at 0, 6, 12, and 16 weeks from all qualified animals and 3D renderings of the scans were used to evaluate the bone volume fraction (BVF) at all time-points.

To analyze the defects, the datasets were rotated using a custom script (ISQ Align) created by a Scanco professional on the Scanco MicroCT V6.1 software. Using three points around the defect, the script can realign the dataset to a new XY plane, allowing the whole circular defect to be visible within one image (Figure 2). Using the realigned dataset, a circular region of interest (ROI), 336 pixels by 336 pixels (diameter = 7.056 mm), was created and spanned 100 slices (100 pixels = 2.1 mm) for a total ROI volume of 82.11 mm^3. This ROI is used to determine the BVF and captures the center of the defect, excluding any natural bone that may be interrupting the 8.0 mm defect, and extends from the above the defect (outside the skull) to below the defect (inside the skull). Micro CT images at 16 weeks were used to calculate the bone bridging score adopted from Patel [20]. A score of zero equating to no bone growth and a score of four indicating complete bone bridging between two sites of the defect. The images were evaluated by 7 observers who were blinded to the conditions.

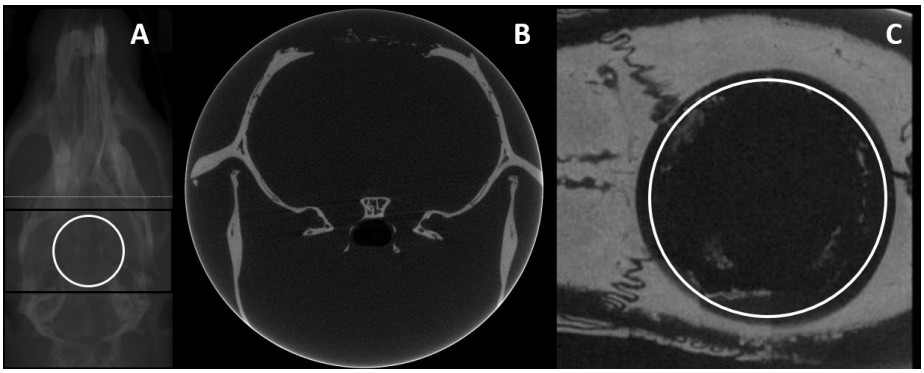

Figure 2: Scout-view/x-ray of rat calvaria showing 8mm defect (white circle) and scanning region (black rectangle) (A). Single slice MicroCT image showing defect (B). Single slice MicroCT image after data set is rotated, showing ROI used for analysis (white circle) (C).

Histological Analysis

At 16 weeks post-surgery the animals were sacrificed. The surgical area was opened and the defect with its surrounding bone removed, photographed, and then fixed in Neutral Buffered Formalin 10% for 24 hours. Thereafter, the sections were decalcified in 12.5% Ethylenediaminetetraacetic acid (EDTA) with the pH adjusted to 6.0-7.5 using sodium hydroxide (NaOH) for two weeks then processed and paraffin imbedded for histology. Sections 6µm thick were stained with hematoxylin and eosin (H&E) and with Masson Trichrome. Four sections of each sample (a total of 24 sections per group) were examined under light microscopy and scored histologically using a modified grading system [24] based on our project specificity. The graded parameters and their possible scores are listed in Table 1. The higher scores indicated more bone regeneration.

Bone formation	**Bone maturity**	**Bone bridging**	**Bone trabeculae**
0-Absent	0- Absent	0-Absent	0-Absent
1-Present at the periphery	1-Mostly immature	1-Incomplete	1-Present at the periphery
2- Present centrally	2-Mostly mature	2-Complete	2- Present centrally
3-Present centrally and at the periphery			3-Present centrally and at the periphery
Haversian Canal	**Inflammation**	**Granulation tissue**	**Neovascularization**
0-Absent	0-Present	0-Present	0-Absent
1-Present at the periphery	1-Absent	1-Absent	1-Present at the periphery
2- Present centrally			2- Present centrally
3-Present centrally and at the periphery			3-Present centrally and at the periphery

Table 1: Shows the parameters used to quantify the histological findings from H&E stained whole sections using 4 sections of each sample.

Statistical Analysis

Bridging scores and histological grading where compared between groups using a student's T-test assuming equal variance. For the bone volume fraction a longitudinal analysis of all outcome measures across time was performed using generalized estimating equation (GEE) modeling. This modeling technique was chosen due to its robust ability to handle data, regardless of whether it met the assumption of normality. Additionally, GEE allowed for the clustered analysis of all observations that had been collected longitudinally and accounted for any missing data that may have been lost to follow-up. All observations were analyzed using maximum likelihood estimations. Models included time and group as fixed effects. All parameter estimates from the GEE models were reported as means and with standard errors. Post-hoc pairwise comparisons were used to analyze within group differences over time as well as between group differences at each time point. Bonferroni correction was used to adjust for multiple pairwise comparisons. Statistical significance was defined as $p \leq 0.05$. All analyses were performed with SPSS, version 23.0 (IBM Corp., Armonk, NY).

Results

Morphometric Analysis

Evaluation of the bone regeneration was performed periodically for 16 weeks. The critical size defect was monitored *in vivo* by micro CT starting within the first few days after surgery and then after 6,12 and 16 weeks of the surgery. Micro CT images showed and increased bone filing of the defect in all groups and is more prevalent in the two experimental groups (CNF and CNF+BMSCs). Bone regeneration is shown as a decrease in the defect size as well as presence of new bone material within the defect (Figure 3).

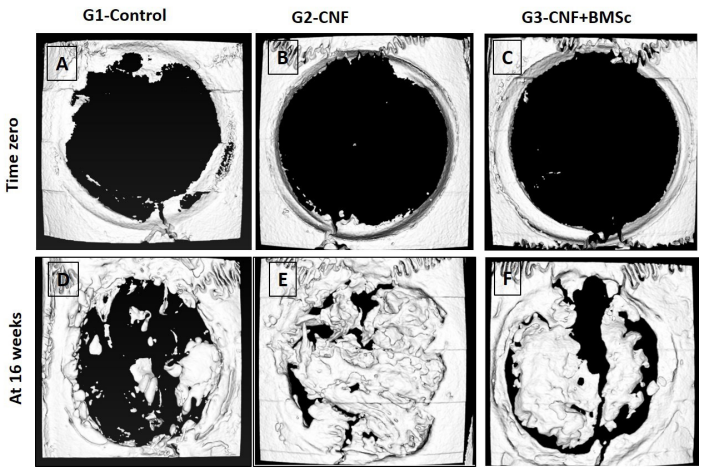

Figure 3: Top view of the 3D micro CT images showing the created defects at time points zero and 16 weeks for all group.

Bone bridging scores at the end of the experiment were higher in the experimental groups with statistically significant differences noted between CNF and the control (p=0.008) and CNF+BMSCs and the control (p=0.049). There were no differences between the experimental groups (p=0.16). A plot representation of the results is shown in Figure 4.

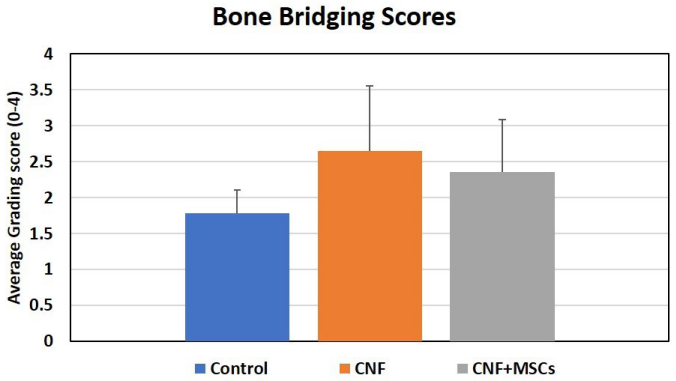

Figure 4: A graphic representation of the bone bridging scores obtained from the top view of the 3D micro CT images for all groups at 16 weeks' time point.

Bone volume fraction values obtained from 3D rendering of the scans were compared within the same group across time and between groups at each time point. Statistically significant results ($p<0.01$) were observed between time zero, 6,12 and 16 weeks for all groups. When comparing between groups the only significant difference was found between G1 vs G2 (p= 0.001, p=0.005 and p=0.006 at 6, 12 and 16 weeks respectively), a plot of the results is shown in Figure 5.

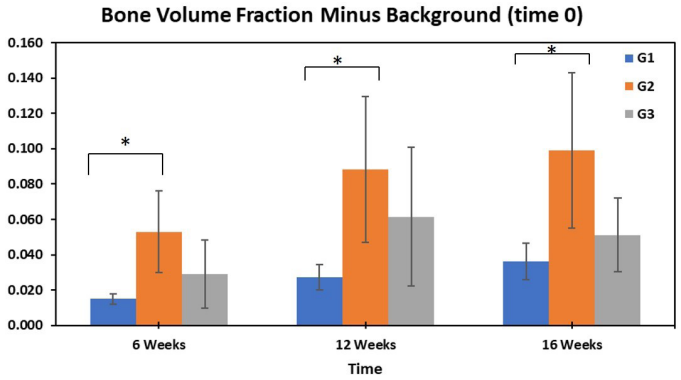

Figure 5: Graph representation of the BVF results, Error bars indicate 95% confidence intervals, * indicates significant difference.

Histological Analysis

Histological evaluation was performed on the decalcified samples. H&E sections were evaluated qualitatively and semi quantitatively for the presence, maturity of the newly formed bone and for signs of inflammatory response. The control group had lower amounts of bone islands within the defect and it was mostly filled with fibrotic tissue. Both CNFs alone and CNF with MSCs groups showed larger amounts of new mature bone with Haversian canals observed and blood vessels within the lamellae of the new bone. Degradation of the nanofibers was observed, and some remnants were visualized by H&E and Trichrome in both experimental groups (Figure 6).

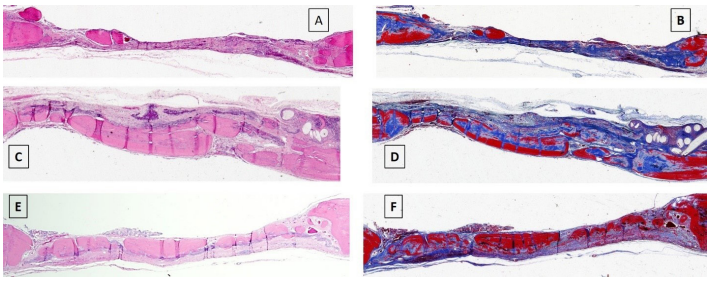

Figure 6: Representative decalcified and paraffin embedded stained samples capturing the whole defect using PathScan at 40x magnification. Left panel is Hematoxylin & Eosin showing bone in pink and collagen in purple color. The right panel is Masson's trichrome stain showing the bone in red and the collagen in blue color. Group 1 control (A&B), Group 2 CNF (C&D) and Group 3 CNF+BMSCs (E&F).

Results from histological grading of the defect were evaluated using unpaired two tailed Student's T-test with equal variance and showed statistically significant difference with $p<0.001$ for G1 vs G2 and for G1 vs G3 but not for G2 vs G3($p=0.382$), results are plotted and shown in (Figure 7).

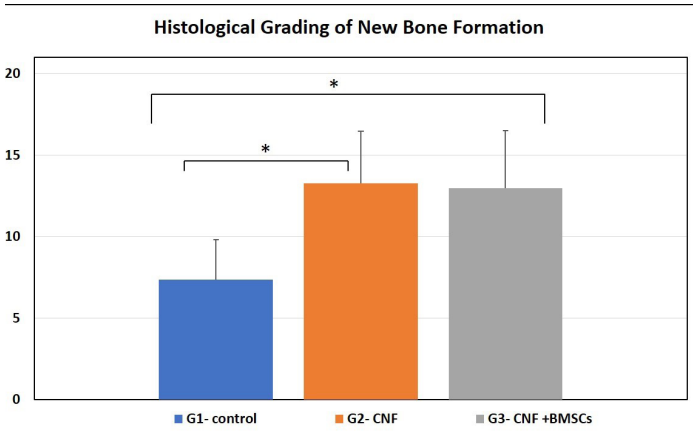

Figure 7: Graphical representation of the histological grading of the decalcified sections, * indicates significance.

Discussion

The objective of this study was to evaluate the effectiveness of type I crosslinked collagen nanofiber sheets and nanofibers seeded with bone marrow stromal cells on healing a critical sized defect in the rat calvaria *in vivo*. The CNFs alone or in combination with BMSCs prevented fibrotic tissue ingrowth into the defect and enhanced the natural healing process.

Over the 16 weeks of study micro-CTs demonstrated increased bone filling of the defect over time in all groups but the experimental groups had more prominent and larger bony areas (Figure 3). The BVF analysis showed that new bone formation was most prominent in the G2 group (CNF) with statistical significant differences from the control at all time points (Figure 5). Interestingly, no significant differences were noted between the G2 and G3 groups indicating that the current method of applying BMSCs did not enhance the positive effect of the collagen nanofiber. The analysis of the 2-D micro CT images showed larger bone coverage areas in both experimental groups (CNF, CNF+BMSCs) that was statistically different from the control (Figure 4). Histological findings supported the micro CT results and the qualitative analysis showed more bone regeneration for both experimental groups (Figures 6 & 7). These *in vivo* findings demonstrated the importance of collagen nanofibers in recruiting local progenitor cells and directing their differentiation into bone forming cells.

The stimulatory effect of various forms of collagen on the differentiation of BMSCs into bone cells has been confirmed in-vitro within honeycomb scaffolds [10] gels [11] and nanofibers [12]. Some *in vivo* studies used collagen blends with beta tricalcium phosphate and compared it to Bio-Oss Collagen [25], have shown improvement in bone regeneration that they related to the effect of beta-TCP. Other group investigated electrospun fibers made from collagen and polylactic acid (PLLA) blend, they showed that this combination enhanced the function of PLLA relative to control, but complete coverage of the defect was not observed [26]. We used pure crosslinked electrospun collagen nanofibers with or without BMSCs and our findings indicated that the addition of BMSCs did not provide additional cues. We believe that the observed effect can be related to the physicochemical nature of the implanted nanofiber matrix. The chemical composition, size and porosity of these nanofibers resembled the host's extracellular matrix. This in turn provided physical and chemical cues that stimulated host stem cells growth and differentiation. Additionally, we believe that the crosslinking of the nanofibers prolonged their degradation time for the length of the experiment (16 weeks) and this provided continuous stimulation. The basis for combining BMSCs with collagen nanofibers was partly due to our previous in-vitro study where we showed that BMSCs survived and differentiated into functional osteoblasts after 3 weeks of culture [12] and we expected that this would further stimulate bone regeneration. Possible reasons why this did not hold true for this *in vivo* experiment could be due to lack of adequate nutrients for the BMSCs immediately after implantation, the change in the behavior of the cells when implanted *in vivo* (like loss of their multipotent characteristic), and perhaps the cell coverage and distribution within the nanofibers masked or modified some cues within the collagen structure.

There were some limitations herein; within the same group we observed variation in patterns of bone filling. In some defects the bone would grow from the periphery and in other the growth appeared to start randomly. We theorize that this limitation could be corrected by increasing our groups sample size. Also due to the small sample size the effect of crosslinking and nanofibers alignment on the mechanical properties after implantation was not tested. Another limitation is the methodology of analysis using the micro CT images. Applying the ROI shape in the same spot every time was quite difficult due software limitations and due to variations in animal positioning during imaging. One more limitation is that in this work we did not perform any viability testing, and this can be corrected in future studies by tagging the implanted cell and follow their fate *in vivo*.

In conclusion we showed that type I crosslinked collagen nanofiber sheets allowed separation of the critical sized calvarial defect from the surrounding tissues. The collagen nanofiber sheets prevented or minimized fibrotic tissue invasion and enhanced the natural healing process with the presence of mineralizing cells within the defect. Adding bone marrow stromal cells did not provide any additional cues for additional bone healing. We recommend additional investigation into the effects of BMSCs by adding the cells immediately during implantation of the nanofibers and using specific identifying markers to follow their differentiation.

Acknowledgement

The authors would like to thank the pathology department at Ascension Providence Hospital for providing guidance in choosing the parameters for the histological analysis. Part of this work was supported by the Research Department at Saint John Hospital and Medical Center Southfield, MI. The authors declare that they have no competing interests. All the data needed to evaluate the conclusions made in this paper are present in the paper. Additional data may be requested from the authors. Parts of this work was presented at the Michigan Orthopaedic Society (MOS June 2018 in Mackinac Island), Orthopaedic Trauma Association (OTA October 2018 in Kissimmee, Orlando), American Association of Hip and Knee Surgeries (AAHKS November 2019 in Dallas) and American Academy of Orthopedic Surgeons (AAOS March 2019 In Las Vegas).

References

1. Ahmad Nassr, Mustafa H Khan, Mir H Ali, et al. Donor-site complications of autogenous nonvascularized fibula strut graft harvest for anterior cervical corpectomy and fusion surgery: experience with 163 consecutive cases. The Spine Journal. 2009; 9: 893-898.
2. David H Kim, Richard Rhim, Ling Li, et al. Prospective study of iliac crest bone graft harvest site pain and morbidity. The Spine Journal. 2009; 9: 886-892.
3. W F Young, R H Rosenwasser. An early comparative analysis of the fibular allograft versus autologous iliac crest graft for interbody fusion after anterior cervical discectomy. Spine. 1993; 18: 1123-1124.
4. W Grossman, W C Peppelman, J A Baum, et al. The use of freeze-dried allograft in anterior cervical fusion. Spine. 1992; 17: 565-569.
5. Randolph C. Bishop, Karen A. Moore and Mark N. Hadley. Anterior cervical interbody fusion using autogeneic and allogeneic bone graft substrate: a prospective comparative analysis. J Neurosurg. 1996; 85: 206-210.
6. Shu-Tung Li. "Biologic Biomaterials: Tissue-Derived Biomaterials (Collagen)." The Biomedical Engineering Handbook: Second Edition. CRC Press LLC, 2000
7. Basak E Uygun, Sarah E Stojsih, Howard W T Matthew. Effects of immobilized glycosaminoglycans on the proliferation and differentiation of mesenchymal stem cells. Tissue Engineering, Part A: Tissue Engineering. 2009; 15: 3499-3512.
8. Jiang Hu, Kai Feng, Xiaohua Liu, et al. Chondrogenic and osteogenic differentiations of human bone marrow-derived mesenchymal stem cells on a nanofibrous scaffold with designed pore network. Biomaterials. 2009; 30: 5061-5067.
9. Christoffer K Abrahamsson, Fan Yang, Hyoungshin Park, et al. Chondrogenesis and mineralization during in vitro culture of human mesenchymal stem cells on three-dimensional woven scaffolds. Tissue Engineering, Part A: Tissue Engineering. 2010; 16: 3709-3718.
10. Joseph George, Yoshinori Kuboki, Teruo Miyata. Differentiation of Mesenchymal Stem Cells into Osteoblasts on Honeycomb Collagen Scaffolds. Biotechnology and Bioengineering. 2006; 95: 404-411.
11. Chamieh F, Collignon AM, Coyac BR, et al. Accelerated craniofacial bone regeneration through dense collagen gel scaffolds seeded with dental pulp stem cells. Sci Rep. 2016; 6: 38814.
12. Bou-Akl T, Miller R, VandeVord P. Collagen Nanofibers Induce Spontaneous Osteogenic Differentiation of Rat Bone Marrow Stromal Cells. Jacobs Journal of Bone Marrow and Stem Cell Research. 2015; 1: 003.
13. Ascenzi A. Bonucci E. "The Tensile Properties of Single Osteons", Anatomical Record. 1967; 158: 375-386.
14. Evans F G. Factors affecting the mechanical properties of bone. Bull N Y Acad Med. 1973; 49: 751-764.
15. Kato YP, Christiansen DL, Hahn RA, et al. Mechanical properties of collagen fibres: A comparison of reconstituted and rat tail tendon fibres. Biomaterials. 1989; 10: 38-42.
16. Olde Damink LH, Dijkstra PJ, van Luyn MJ, et al. Cross-linking of dermal sheep collagen using a water-soluble carbodiimide. Biomaterials. 1996; 17: 765-773.
17. Caruso AB, Dunn MG. Functional evaluation of collagen fiber scaffolds for ACL reconstruction: Cyclic loading in proteolytic enzyme solutions. J Biomed Mater ResA. 2004; 69: 164–171.
18. Bou-Akl T, Banglmaier R, Miller R, et al. Effect of crosslinking on the mechanical properties of mineralized and non-mineralized collagen fibers. J Biomed Mater Res Part A. 2013: 101A: 2507-2514. Elsdale T, Bard J. Collagen substrata for studies on cell behavior. J Cell Biol. 1972; 54: 626-637.
19. Matthews JA, Wnek GE, Simpson DG, et al. Electrospinning of collagen nanofibers. Biomacromolecules. 2002; 3: 232-238.
20. Acharya M, Arumugam GK, Heiden PA. Dual Electric Field Induced Alignment of Electrospun Nanofibers. Macromolecular Materials and Engineering. 2008; 293: 666-674.
21. Javazon EH, Colter DC, Schwarz EJ, et al. Rat marrow stromal cells are more sensitive to plating density and expand more rapidly from single-cell-derived colonies than human marrow stromal cells. Stem Cells. 2001; 19: 219-225.
22. Spicer PP, Kretlow JD, Young S, et al. Evaluation of bone regeneration using the rat critical size calvarial defect. Nat Protoc. 2012; 7: 1918-1929.
23. Zarana S Patel, Simon Young, Yasuhiko Tabata, et al. Dual Delivery of an Angiogenic and an Osteogenic Growth Factor for Bone Regeneration in a Critical Size Defect Model. Bone.

2008; 43: 931-940.
24. Lucaciu O, Gheban D, Soriţau O, et al. Comparative assessment of bone regeneration by histometry and a histological scoring system / Evaluarea comparativă a regenerării osoase utilizând histometria și un scor de vindecare histologică, Revista Romana de Medicina de Laborator, 2015; 23: 31-45.
25. Maciel Juceleia, Momesso Gustavo Antonio Correa, Ramalho-Ferreira, et al. Bone Healing Evaluation in Critical-Size Defects Treated With Xenogenous Bone Plus Porcine Collagen. Implant Dentistry. 2017; 26: 296-302.
26. E Kato, J Lemler, K Sakurai, et al. Biodegradation Property of Beta-Tricalcium Phosphate-Collagen Composite in Accordance with Bone Formation: A Comparative Study with Bio-Oss Collagen® in a Rat Critical-Size Defect Model Clin. Implant Dent. Rel. Res. 2014; 16: 202-211.
27. Schofer M D, Tünnermann L, Kaiser H, et al. Functionalisation of PLLA nanofiber scaffolds using a possible cooperative effect between collagen type I and BMP-2: impact on colonization and bone formation *in vivo*. Journal of materials science. Materials in Medicine. 2012; 23: 2227-2233.